Parameter estimation and change-point detection from Dynamic Contrast Enhanced MRI data using stochastic differential equations

Charles-André Cuenod[a,b], Benjamin Favetto[c], Valentine Genon-Catalot[c], Yves Rozenholc[c], Adeline Samson[c]

[a] *Université Paris Descartes, HEGP Radiology, France*
[b] *LRI at PARC, INSERM U970*
[c] *Université Paris Descartes, MAP5, UMR CNRS 8145, France*

Abstract

Dynamic Contrast Enhanced imaging (DCE-imaging) following a contrast agent bolus allows the extraction of information on tissue micro-vascularization. The dynamic signals obtained from DCE-imaging are modeled by pharmacokinetic compartmental models which integrate the Arterial Input Function. These models use ordinary differential equations (ODEs) to describe the exchanges between the arterial and capillary plasma and the extravascular-extracellular space. Their least squares fitting takes into account measurement noises but fails to deal with unpredictable fluctuations due to external/internal sources of variations (patients' anxiety, time-varying parameters, measurement errors in the input function, etc). Adding Brownian components to the ODEs leads to stochastic differential equations (SDEs). In DCE-imaging, SDEs are discretely observed with an additional measurement noise. We propose to estimate the parameters of these noisy SDEs by maximum likelihood, using the Kalman filter. In DCE-imaging, the contrast agent injected in vein arrives in plasma with an unknown time delay. The delay parameter induces a change-point in the drift of the SDE and ODE models, which is estimated also. Estimations based on the SDE and ODE pharmacokinetic models are compared to real DCE-MRI data. They show that the use of SDE provides robustness in the estimation results. A simulation study confirms these results.

Keywords: Angiogenesis, DCE-imaging, Kalman Filter, Parameter estimation, Stochastic Differential Equation

1. Introduction

Tissue micro-vascularization and angiogenesis can now be studied in vivo by several Dynamic Contrast Enhanced Imaging (DCE-imaging) techniques. These techniques are increasingly used in the medical imaging of brain, heart and cancer [1, 2, 3, 4]. DCE-imaging follows a bolus of contrast agent injected during a sequential imaging acquisition with Computed Tomography, Magnetic Resonance Imaging or Ultrasound imaging (DCE-CT, DCE-MRI or DCE-US) [5, 1]. Recent experimental and clinical studies have shown that DCE-imaging can assess tumor aggressiveness and monitor the *in vivo* effects of treatments [6, 7, 8, 9].

Four quantities are usually used to characterize vasculature: the tissue blood flow (perfusion), the permeability surface area, the tissue blood fractional volume and the tissue extravascular-extracellular space fractional volume [10, 11]. Sequential imaging data are related to these parameters through pharmacokinetic compartment models, that describe the exchanges of the contrast agent between a central compartment (plasma) and a peripheral compartment (extracellular space or interstitial water). Recently, the need to integrate the Arterial Input Function (AIF) in the model to estimate microcirculation parameters more accurately has been emphasized [12, 13, 14]. However, deterministic pharmacokinetic models generally fail to capture the random fluctuations due to external or internal environmental causes (patients' moves, anxiety, small random variations of the microvascularization parameters along time, measurement error in the AIF, baseline estimation error, etc) which occur in supplement of the measurement noise due to electronic devices. These additional sources of variations are unpredictable and thus impossible to model in a deterministic way. Spatial averaging or large regions of interest are generally considered to minimize the failure of deterministic models on voxel data [14]. This implies mixing or averaging dynamics which may be heterogeneous, and leads to inaccurate parameter estimation.

In this paper, we propose to model the unexplained sources of variations by adding random components to the compartment differential system. This approach is applied to each voxel separately. More precisely, we consider a pharmacokinetic model describing the kinetics of the contrast agent in the voxel with two compartments (plasma and interstitial water). This deterministic model is transformed into a stochastic differential system by adding a Brownian motion to each differential equation. Observations obtained from

DCE-imaging are noisy measurements of the total contrast agent quantity described by the stochastic differential system. The measurement noise differs from the random variations added to the pharmacokinetic model. It is due to the precision of the recording experiments and is thus an uncorrelated noise. Parameter estimation in this model is complex. [15] propose a way to compute the exact likelihood using the Kalman filter recursion when the AIF is constant. They study the asymptotic properties of the maximum likelihood estimator and illustrate their approach on simulated data.

The aim of this paper is to extend their approach when the AIF is not constant. The contrast agent is injected in vein and arrives in plasma after an unknown time delay δ (Bolus Arrival Time). Thus the delay parameter δ is a time where a change occurs in the drift of the SDE and ODE models. This yields to a the model including a change-point detection. As proved in [15], the noisy discrete observations taken here is an ARMA(2,2) process. Under some assumptions on the AIF function, we study the method proposed by [16] for estimating the change-point in an ARMA model. We also estimate the microcirculation parameters and the change-point by maximum likelihood. This approach is compared with the classic deterministic model on real data, illustrating the improvement in estimation quality of the SDE model. A simulation study confirms these results. Indeed, the use of a stochastic model stabilizes parameter estimations and provides robustness in the estimation results with respect to special or sensitive data points (e.g. due to patient movements or measurement disturbances). When we remove some special data points, the ODE estimation may change totally while the SDE estimation remains stable. Note that the ODE estimation encounters numerical difficulties due to constraints on the parameters. Such numerical problems are not observed for the SDE estimation under the same constraints.

The article is organized as follows. In Section 2, the data, the deterministic and stochastic differential systems are presented. The estimation methods are described in Section 3. The results of estimation on DCE-MRI data of normal female pelvises are given in Section 4 for both ODE and SDE models. A simulation study is presented in Section 5. The discussion and conclusions are presented in Section 6.

2. Models

2.1. MRI data extraction

The acquisition of the MRI sequence was performed at discrete times $t_0 = 0 < t_1 < \ldots < t_n = T$. Two local sets of voxels were drawn manually on one of the MR images (one in the left iliac artery and the other in the pelvis) and propagated automatically over the entire image sequence. For a given voxel, the gray levels are denoted $(z_0, \ldots, z_n)$. A baseline gray level b_0 is estimated by averaging the first times of the sequence before the injection of the contrast agent. Observations are defined as the gray level differences between the voxel gray levels z_i and the baseline gray level b_0 and are denoted $y_i = z_i - b_0$ for $i = 0, \ldots, n$. The measurements obtained from the arterial voxel after removing the baseline are denoted $(AIF(t_i))_{0 \leq i \leq n}$ (Arterial Input Function). We assume that the gray level variation y_i at time t_i is proportional to the total quantity of contrast agent inside the voxel up to some additive measurement errors due to the acquisition technique. Let $S(t)$ denote the total quantity of contrast agent inside the voxel. The following relation is assumed

$$y_i = S(t_i) + \sigma\varepsilon_i, \tag{1}$$

where (ε_i) are the measurement error random variables, assumed to be Gaussian, centered, standardized, mutually independent and independent of $(S(t))$ and σ is the constant noise level. The whole vector of data is denoted $y_{0:n}$.

2.2. Pharmacokinetic models

Two physiological models are considered to describe the evolution of $S(t)$ within each voxel after the contrast agent injection. They are both derived from the same pharmacokinetic model [10, 11] based on a compartmental analysis (Figure 1). In this model, the contrast agent within a tissue voxel is assumed to be either in the plasma compartment of the micro-vessels (capillaries) or inside the interstitial compartment (extracellular-extravascular space). The contrast agent quantities in a single unit voxel at time t are denoted $Q_P(t)$ and $Q_I(t)$ for plasma and interstitial compartments, respectively. In a single voxel of unit volume, we have $S(t) = Q_P(t) + Q_I(t)$. The contrast agent, a gadolinium chelate, cannot enter red or tissue cells.

The contrast agent is injected in vein at time t_0, transits in the artery and arrives in plasma, with a tissue perfusion flow per unit volume equal to $F_T \geq 0$ (in $\mathrm{ml.min^{-1}.100ml^{-1}}$), proportionally to the concentration in

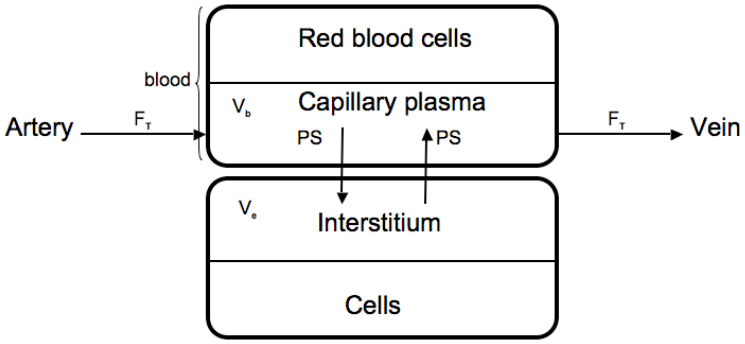

Figure 1: Two-compartment physiological pharmacokinetic model used to describe the distribution of the contrast agent.

the artery $AIF/(1-h)$, where h is the hematocrit rate. The delay with which the contrast agent arrives from the arteries to the plasma (or Bolus Arrival Time) is denoted δ. The contrast agent is eliminated from plasma with the perfusion flow F_T, proportionally to the concentration of contrast agent in plasma $Q_P/(V_b(1-h))$, where $V_b \geq 0$ is the part of whole blood volume (in %). The quantity of contrast agent exchanging from plasma to interstitium is equal to PS times the concentration of contrast agent in plasma $Q_P/(V_b(1-h))$, where PS is the permeability surface area product per unit volume of tissue (in $\text{ml.min}^{-1}.100\text{ml}^{-1}$) and $V_e \geq 0$ is the part of extravascular extracellular space fractional volume (in %). Conversely, the quantity of contrast agent exchanging from interstitium through plasma is equal to PS times the concentration of contrast agent in interstitium Q_I/V_e. Note that $V_b + V_e \leq 100$. The hematocrit rate h is set to $h = 0.4$. Both t and δ are measured in seconds.

2.3. The ordinary differential pharmacokinetic model (ODE)

Using the pharmacokinetic model presented in Figure 1 and assuming constant rates in the exchanges, [10] propose the following differential equations to model the contrast agent kinetics, called the Ordinary Differential

Equation (ODE) model:

$$\begin{aligned}
\frac{dQ_P(t)}{dt} &= \frac{F_T}{1-h}\, AIF(t-\delta)\mathbf{1}_{[\delta,\infty)}(t) - \frac{PS}{V_b(1-h)}Q_P(t) + \frac{PS}{V_e}Q_I(t) \\
&\quad - \frac{F_T}{V_b(1-h)}Q_P(t), \qquad (2) \\
\frac{dQ_I(t)}{dt} &= \frac{PS}{V_b(1-h)}Q_P(t) - \frac{PS}{V_e}Q_I(t)
\end{aligned}$$

where $\mathbf{1}_{[\delta,\infty)}(t)$ is the binary function equal to 1 when t belongs to the interval $[\delta, \infty)$ and 0 otherwise. We assume that no contrast agent exists inside the body before acquisition. Hence the initial conditions $Q_P(t_0) = Q_I(t_0) = 0$ and $AIF(t_0) = 0$ hold, with $t_0 = 0$. The delay δ corresponds to a change-point in the model. This model only requires the biological parameters of interest $(F_T, V_b, PS, V_e, \delta)$ and the knowledge of $AIF(t)$. Given a set of parameters and the AIF, Q_P and Q_I are deterministic functions of time.

2.4. The stochastic differential pharmacokinetic model (SDE)

The ODE model (2) is a simplified model of the true contrast agent pharmacokinetics. For example, it fails to capture measurement errors in the arterial input function, or random fluctuations along time in the microcirculation parameters. These variations are unpredictable. Our main hypothesis is that a more realistic modeling can be obtained by a stochastic approach. We introduce a stochastic version of the ODE model, by adding random components to each equation:

$$\begin{aligned}
dQ_P(t) &= \left(\frac{F_T}{1-h}\, AIF(t-\delta)\mathbf{1}_{[\delta,\infty)}(t) - \frac{PS}{V_b(1-h)}Q_P(t) + \frac{PS}{V_e}Q_I(t)\right. \\
&\quad \left. - \frac{F_T}{V_b(1-h)}Q_P(t)\right) dt + \sigma_1 dW_t^1, \qquad (3) \\
dQ_I(t) &= \left(\frac{PS}{V_b(1-h)}Q_P(t) - \frac{PS}{V_e}Q_I(t)\right) dt + \sigma_2 dW_t^2
\end{aligned}$$

where (W_t^1) and (W_t^2) are two independent real-valued standard Brownian motions, and σ_1, σ_2 are the standard deviations of the random perturbations, also called volatility parameters. The initial conditions are the same as above.

Although we use the same notations as in (2), given a set of parameters and the AIF, the solutions Q_P and Q_I of (3) are stochastic processes.

This model is called the Stochastic Differential Equation (SDE) model. This SDE is time-inhomogeneous due to the AIF. Its expectation corresponds to the ODE model, which includes the change-point δ. Therefore SDE and ODE parameters have the same physiological interpretation. The random part of the SDE represents the random fluctuations around the deterministic ODE. In particular, the random perturbation $\sigma_1 dW_t^1$ takes into account the measurement noise of the arterial input function among other sources of variations.

This model can be written in a matrix form. Let denote $Q(t) = (Q_P(t), Q_I(t))'$, $(W(t) = (W_1(t), W_2(t))', t \geq 0)$ a standard 2-dimensional Brownian motion where X' denotes the transposed matrix of X. The SDE system (3) is written

$$dQ(t) = (GQ(t) + F(t))dt + \Sigma dW(t), \quad Q(0) = (0,0)' \tag{4}$$

$$G = \begin{pmatrix} -\lambda - \beta & \beta \\ \lambda & -k \end{pmatrix}, \quad \Sigma = \begin{pmatrix} \sigma_1 & 0 \\ 0 & \sigma_2 \end{pmatrix}, \quad F(t) = \begin{pmatrix} \alpha AIF(t-\delta)\mathbf{1}_{[\delta,\infty)}(t) \\ 0 \end{pmatrix},$$

with a change-point in the drift function at time $t = \delta$ and where $\alpha, \beta, \lambda, k$ are related to the biological parameters by the relations

$$\alpha = \frac{F_T}{1-h}, \beta = \frac{F_T}{V_b(1-h)}, \lambda = \frac{PS}{V_b(1-h)}, k = \frac{PS}{V_b(1-h)} + \frac{PS}{V_e}.$$

In the following, we consider two models of perturbations, *i.e.* two different volatility matrices Σ. Model SDE 1 corresponds to the case $\sigma_1 \neq \sigma_2 \neq 0$ and model SDE 2 to $\sigma_2 = 0$, corresponding to these volatility matrices, respectively:

$$\Sigma_1 = \begin{pmatrix} \sigma_1 & 0 \\ 0 & \sigma_2 \end{pmatrix}, \quad \Sigma_2 = \begin{pmatrix} \sigma_1 & 0 \\ 0 & 0 \end{pmatrix}. \tag{5}$$

3. Estimation methods

Estimation in ODE is classically performed with standard least squares in Section 3.1. Estimation in SDE models is complex due to the change-point detection δ and is presented in Section 3.2.

3.1. Estimation in the ODE model

We aim at estimating the parameters of interest $(F_T, V_b, PS, V_e, \delta, \sigma)$ of the ODE model observed with additive noise. The parameters $(F_T, V_b, PS, V_e, \delta)$

are classically estimated by standard least squares by minimizing

$$\sum_{i=0}^{n}(y_i - S(t_i))^2 = \sum_{i=0}^{n}(y_i - Q_P(t_i) - Q_I(t_i))^2 \tag{6}$$

with respect to $(F_T, V_b, PS, V_e, \delta)$ where $(Q_P(t), Q_I(t))$ are the solutions of (2). A plug-in of these estimated parameters in (2) provides an estimation of the functions $Q_P(t)$, $Q_I(t)$ and $S(t)$ denoted $\hat{Q}_P^{\text{ODE}}(t)$, $\hat{Q}_I^{\text{ODE}}(t)$ and $\hat{S}^{\text{ODE}}(t)$, respectively. To estimate σ, we set

$$\hat{\sigma} = \sqrt{\frac{1}{n-4}\sum_{i=0}^{n}(y_i - \hat{S}^{\text{ODE}}(t_i))^2}. \tag{7}$$

For short, we set $\phi = (F_T, V_b, PS, V_e, \delta, \sigma)$ and $\hat{\phi} = (\hat{F}_T, \hat{V}_b, \hat{PS}, \hat{V}_e, \hat{\delta}, \hat{\sigma})$. Standard deviations for each parameter estimate except δ are obtained numerically through the Fisher information matrix. Indeed, the likelihood is not derivable with respect to δ.

3.2. Estimation in the SDE model

For the statistical parameters in the SDE model, we set $\theta = (F_T, V_b, PS, V_e, \sigma_1, \sigma_2, \sigma)$ the parameters vector where δ is omitted. The discretized process $(S(t_i))$ is a hidden Markov chain which yields to a Hidden Markov Model (HMM) for $(y_{0:n}, S(t_i))$. Due to the SDE model and assumptions, $(S(t))$ is a Gaussian process and $y_{0:n}$ is a Gaussian vector. More precisely, in equation (4), matrix G is diagonalizable. Let us denote D the corresponding diagonal matrix of eigenvalues and P the matrix of eigenvectors. Let $X(t) = P^{-1}Q(t)$ and $\Gamma = P^{-1}\Sigma$. The observation times are equally spaced. We denote $t_{i+1} - t_i = \Delta$ and $X_i = X(t_i)$. Thus, the discrete-time evolution system is

$$\left\{ \begin{array}{rcl} X_i & = & AX_{i-1} + B_i + \eta_i, \quad \eta_i \sim \mathcal{N}(0, R_i) \\ y_i & = & HX_i + \sigma\varepsilon_i \end{array} \right. \tag{8}$$

with $H = (1,1)P$, $A = e^{D\Delta}$, $R_{i+1} = \int_{(i-1)\Delta}^{i\Delta} e^{D(t_i - s)}\Gamma\Gamma' e^{D'(t_i - s)}ds$ and

$$B_i = \left\{ \begin{array}{ll} 0 & \text{if} \quad 0 \leq i\Delta \leq \delta \\ \int_{(i-1)\Delta}^{i\Delta} e^{D(t_i - s)}P^{-1}F(s)ds & \text{if} \quad \delta < i\Delta \end{array} \right.$$

By introducing the auto-regressive process $Z_i = AZ_{i-1} + \eta_i$, the change-point can be isolated in the system. Formally, system (8) is equivalent in distribution to the following set of equations

$$\left\{ \begin{array}{rcl} Z_i &=& AZ_{i-1} + \eta_i, \quad \eta_i \sim \mathcal{N}(0, R_i) \\ \tilde{y}_i &=& HZ_i + \sigma\varepsilon_i, \\ y_i &=& c_i + \tilde{y}_i, \end{array} \right.$$

with

$$C_i = AC_{i-1} + B_i = A^i \int_0^{i\Delta} e^{-Ds} P^{-1} F(s) ds \tag{9}$$

and $c_i = HC_i$. Thus $c_i = 0$ for $i\Delta \leq \delta$ and $c_i \neq 0$ for $i\Delta > \delta$. Remark that as in [15], process (Z_i) is an AR(1) two-dimensional process and $\tilde{y}_i$ is an ARMA(2,2) process.

We assume that the delay δ is such that $\delta = j^\star\Delta$, with $j^\star \in \mathbb{N}$. The maximum likelihood estimators of $(\theta, j^\star)$ are defined as

$$(\hat{j^\star}, \hat{\theta}) = \arg\max_{j,\theta} L(j, \theta, y_{0:n})$$

where the log-likelihood $L(j, \theta, y_{0:n})$ can be exactly computed by

$$\begin{array}{rcl} L(j, \theta, y_{0:n}) &=& \displaystyle\sum_{i=1}^{j} \frac{(y_i - H\hat{Z}_i^-)^2}{HP_i^-H' + \sigma^2} + \log(HP_i^-H' + \sigma^2) \\ && \displaystyle - \sum_{i=j+1}^{n} \frac{(y_i - H\hat{Z}_i^- - c_j)^2}{HP_i^-H' + \sigma^2} + \log(HP_i^-H' + \sigma^2). \end{array}$$

where $\hat{Z}_i^-$ and P_i^- are the expectation and variance of the prediction distribution $p(Z_i|y_{0:i-1})$ computed by the Kalman algorithm [see 15, for more details]. From a practical point of view, we propose an estimation method in two steps. We first maximize $L(j, \theta, y_{0:n})$ in θ for each j, yielding to $\hat{\theta}(j) = \arg\max_\theta L(j, \theta, y_{0:n})$. Then $j^\star$ is estimated by $\hat{j^\star} = \arg\max_j L(j, \hat{\theta}(j), y_{0:n})$. In Section 4, we compute the maximum likelihood estimators of all parameters on real data assuming that the AIF is piecewise constant. Figure 2 illustrates the second step of this two-step method. The value of the maximum $L(j, \hat{\theta}(j), y_{0:n})$ of the log-likelihood $L(j, \theta, y_{0:n})$ for a given value j is fitted with respect to different values of j.

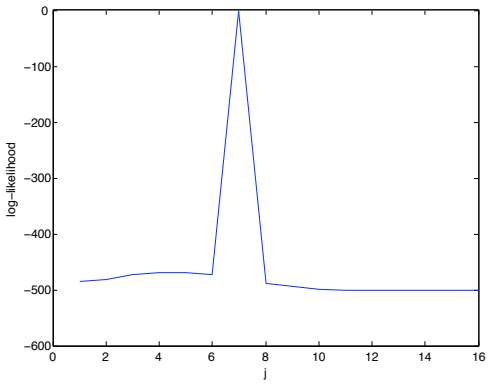

Figure 2: Estimation of the change-point $\delta = j^\star\Delta$ in model SDE 1 for the first real dataset. Maximum $L(j, \hat{\theta}(j), y_{0:n})$ of the log-likelihood $L(j, \theta, y_{0:n})$ for a given value j is fitted with respect to different values of j. Estimator $\hat{j}^\star$ is the value of j which maximizes $L(j, \hat{\theta}(j), y_{0:n})$.

3.2.1. Assumptions on the AIF

The simultaneous theoretical study of maximum likelihood estimators $\hat{j}^\star$ and $\hat{\theta}$ is difficult. To obtain theoretical properties on the change-point estimation in this model, we propose a separate study. We introduce a least squares estimator of the change-point inspired by [16]. We study its asymptotic properties under different assumptions on the AIF. This method is not implemented here as we believe that the exact MLE is better. Nevertheless, it illustrates the asymptotic properties of change-point estimation. An analogous behavior is expected for the MLE.

We assume that the AIF is piecewise constant: there exist known numbers $(a_j)_{j=1,\dots,n}$ (measured in an artery voxel) such that

$$AIF(t) = \sum_{j=1}^{n} a_j \mathbf{1}_{[(j-1)\Delta, j\Delta[}(t).$$

In that case, from equations (4) and (9), we have

$$C_i = \sum_{j=1}^{i-j^\star} a_j e^{(i-j-j^\star)\Delta D}(I - e^{-\Delta D})D^{-1}P^{-1}(\alpha \;\; 0)'.$$

But $e^{(i-j-j^\star)\Delta D}$ is close to 0 if $j \leq i - j^\star - 2$.

Now we distinguish two conditions which correspond to two phases of the experiment (see Figure 3).

(A1) Linear assumption on AIF We consider that AIF has a linear growth ($a_j = j\Delta$), which is realistic in the first phase of the experiment. In this first phase, c_i can be approximated by $c_i = \mu_0 + \mu_1(i - j^\star)$ where μ_0 and μ_1 are two unknown parameters depending on θ and Δ.

(A2) Constant assumption on AIF We consider that AIF is constant, which is realistic after the peak of injection. Then c_i can be approximated by an unknown constant μ_2.

3.2.2. Change-point estimator

Under (A1), the system of observations is

$$\left\{ \begin{array}{rcl} Z_i & = & AZ_{i-1} + \eta_i, \quad \eta_i \sim \mathcal{N}(0, R_i) \\ \tilde{y}_i & = & HZ_i + \sigma\varepsilon_i \\ y_i & = & \mu_0 + \mu_1(i - j^\star)\mathbf{1}_{i>j^\star} + \tilde{y}_i \end{array} \right.$$

[16] considers a similar problem with an ARMA process $(\tilde{y}_i)$ but with a constant change in the drift $\mu_0 + \mu_1\mathbf{1}_{i\geq j^\star}$. The next proposition shows that our problem reduces to that case.

***Proposition* 1.** *Consider the process of increments $V_i = y_{i+1} - y_i$ for $1 \leq i \leq n$. We have*

$$V_i = \mu_1\mathbf{1}_{i\geq j^\star} + U_i \tag{10}$$

with U_i an ARMA(2,3) process.

Proof. Let $U_i = \tilde{y}_{i+1} - \tilde{y}_i$. Process $(\tilde{y}_i)$ is an ARMA(2,2) process [see 15]. Thus there exist two parameters θ_1, θ_2 and a MA(2) process (ν_i) such that

$$\tilde{y}_i - (\theta_1 + \theta_2)\tilde{y}_{i-1} + \theta_1\theta_2\tilde{y}_{i-2} = \nu_i$$

Therefore

$$U_i - (\theta_1 + \theta_2)U_{i-1} + \theta_1\theta_2U_{i-2} = \nu_i - \nu_{i-1}$$

and $(\nu_i - \nu_{i-1})$ has a MA(3) structure. □

The least-squares change-point estimator studied in [16] can be applied to the process (V_i). Consider $\bar{V}_j$ the mean of the first j observations and $\bar{V}_j^*$ the mean of the last $n - j$ observations which are the usual least squares

estimators of the mean before and after the change-point, *i.e.* μ_0 and μ_1. The corresponding sum of squares of residuals is

$$S_j^2 = \sum_{i=1}^{j}(V_i - \bar{V}_j)^2 + \sum_{i=j+1}^{n}(V_i - \bar{V}_j^*)^2$$

The estimator is defined as follows:

$$\hat{j} = \arg\min_j S_j^2$$

The properties of $\hat{j}$ are studied using the arguments of [16], Proposition 3.

***Proposition* 2.** *Assume that $j^\star = \lfloor n\tau^\star \rfloor$ for $\tau^\star \in (0,1)$ and define $\hat{\tau} = \hat{j}/n$. Then,*

$$\hat{\tau} - \tau^\star = O_P(\frac{1}{\mu_1^2 n}). \tag{11}$$

The fact that τ is estimated faster than θ justifies the two steps estimation approach.

3.2.3. Estimation of microcirculation parameters

We now study the properties of $\hat{\theta}(j)$ where j is fixed at the true value $j^\star$, $\hat{\theta} = \hat{\theta}(j^\star)$, under (A2). The system of observations is

$$\left\{ \begin{array}{rcl} Z_i & = & AZ_{i-1} + \eta_i, \quad \eta_i \sim \mathcal{N}(0, R_i) \\ \tilde{y}_i & = & HZ_i + \sigma\varepsilon_i \\ y_i & = & \mu_2 + \tilde{y}_i \end{array} \right.$$

This reduces to the case treated by [15]. Taking the same parametrization $\theta = (\theta_1, \theta_2, \theta_3, \theta_4, \theta_5, \theta_6, \theta_7)$ such that

$$A = A(\theta) = \begin{pmatrix} \theta_1 & 0 \\ 0 & \theta_2 \end{pmatrix}, \quad R = R(\theta) = \begin{pmatrix} \theta_3 & \theta_5 \\ \theta_5 & \theta_4 \end{pmatrix}, \quad \theta_6 = \mu_2 \quad \text{and} \quad \theta_7 = \sigma,$$

they prove the following proposition:

***Proposition* 3.** *Only six out of the seven parameters are identifiable. Under the assumption that $(\tilde{y}_i)$ is stationary, the maximum likelihood estimators of these six parameters are consistent and asymptotically Gaussian with rate $\sqrt{n}$.*

Therefore, we propose to approximate the standard deviations for each parameter estimate through the Fisher information matrix. This asymptotic approximation is realistic when n is large, which is the case in our application. We propose to compute $\frac{\partial^2}{\partial\theta_i\partial\theta_j} l_{0:n}(\theta)$ with a finite-difference like method, where $l_{0:n}(\theta) = L(j^\star, \theta, y_{0:n})$:

$$\begin{aligned}\frac{\partial^2 l_{0:n}}{\partial\theta_i\partial\theta_j}(\theta) &\approx \frac{1}{4\Delta\theta_i\Delta\theta_j}\left(l_{0:n}(\theta+\Delta\theta_i+\Delta\theta_j) + l_{0:n}(\theta-\Delta\theta_i-\Delta\theta_j)\right.\\ &\quad \left. -l_{0:n}(\theta+\Delta\theta_i-\Delta\theta_j) - l_{0:n}(\theta-\Delta\theta_i+\Delta\theta_j)\right)\end{aligned}$$

where $\Delta\theta_i$ and $\Delta\theta_j$ are small step sizes in the direction of θ_i and θ_j, respectively. The convergence rate of the method is improved by the Richardson method [see 17, for details]. Hence, we can derive an asymptotic confidence interval for θ computing $I_n(\theta) = -\frac{1}{n}\frac{\partial^2}{\partial\theta_i\partial\theta_j} l_{0:n}(\theta)$.

The corresponding estimations $\hat{Q}_P^{\text{SDE}}(t)$, $\hat{Q}_I^{\text{SDE}}(t)$ and $\hat{S}^{\text{SDE}}(t)$ of $Q_P(t)$, $Q_I(t)$ and $S(t)$ are defined as the conditional expectations of $Q_P(t)$, $Q_I(t)$ and $S(t)$ given the observation $y_{0:n}$ and assuming the unknown parameter θ to be equal to $\hat{\theta}$:

$$\hat{Q}_P^{\text{SDE}}(t) = E_{\hat{\theta}}(Q_P(t)|y_{0:n}),\ \hat{Q}_I^{\text{SDE}}(t) = E_{\hat{\theta}}(Q_I(t)|y_{0:n}),\ \hat{S}^{\text{SDE}}(t) = E_{\hat{\theta}}(S(t)|y_{0:n}).$$

These estimated stochastic signals are computed by the smoother algorithm [see 15, for more details]. We also propose to quantify the uncertainty of these estimated signals by computing their 95% confidence intervals.

3.3. Numerical implementation of the two estimation methods

The computation of the ODE mean squares and the SDE likelihood required the integral of the arterial input function, which was approximated using the trapezoidal method: the integral $\int_{t_0}^{t_i} AIF(x)dx$ over the interval $[t_0, t_i]$ was approximated by $\sum_{k=1}^{i}(t_k - t_{k-1})(AIF(t_k) + AIF(t_{k-1}))/2$. The minimization of (6) for the ODE model and the maximization of the likelihood for the SDE models were performed under the constraints:

$$0 \leq PS, F_T; \quad 0 \leq V_b, V_e \leq 100; \quad V_b + V_e \leq 100.$$

The two optimizations were done using the Matlab$^{\text{TM}}$ function `fmincon` available in the toolbox `Optimization` release 2008b, which realizes a constraint optimization. Using this `fmincon` function, we observed that the initial values provided by the user have no influence on the final optimization results.

Therefore, the initial values were arbitrarily chosen as $F_T = 50$, $V_b = 10$, $PS = 10$, $V_e = 10$ for the ODE optimization adding the extra values $\sigma = 5$, $\sigma_1 = 1$ and $\sigma_2 = 0.5$ for the SDE optimization. Computational times were about 4 seconds for the ODE and 20 seconds for the SDE methods, on a Mac Pro 3 Ghz with 7 Go RAM, Mac OS X 10.5 and Matlab$^{\text{TM}}$ Release 2008b.

4. Estimation on real data

DCE-MRI data from a series of normal female pelvises DCE-MRI were used to test and optimize the processing method [18]. For DCE-MRI, a dynamic contrast-enhanced sequence was acquired in the axial plane. A dose of 0.1 mmol.kg^{-1} body weight of DOTA gadolinium was injected intravenously. Images were obtained at 2.4 second intervals for a total of 320 seconds after injection, yielding a total of 130 time frames.

Four datasets were analyzed on a voxel by voxel basis. The ODE and the two SDE models (5) were successively used to estimate the parameters and the associated predicted concentrations. The ODE and SDE residuals were computed as the difference between the observations $y_{0:n}$ and the predictions of the corresponding model. The BIC criteria was computed to compare the four models.

The first dataset is summarized in Table 1 and Figure 3, top figures. Standard deviation of δ is meaningless as the likelihood is not derivable with respect to δ. For this voxel, the ODE and SDE estimates of F_T, V_b, PS, V_e and δ were identical as well as the contrast agent quantity predictions. In that case, the estimates of σ_1 and σ_2 were both very small ($< 10^{-3}$). The standard errors of the microcirculation parameters were slightly greater for the SDE models than for the ODE model. The standard error of σ was systematically close to 0 with the SDE models. BIC was smaller for the ODE model, as it is the most parsimonious model.

For dataset 2, ODE and SDE estimations were statistically different at least for one parameter (F_T) (see Table 2 and Figure 3, bottom figures). The 95% ODE confidence interval of parameter F_T did not contain the SDE estimated values. The estimation of δ was the same for the two SDE models and different for the ODE model. The parameter σ_2 is estimated close to zero ($< 10^{-3}$) in model SDE 1 while σ_1 is different from 0 ($\hat{\sigma}_1^{\text{SDE}} = 1.0$) for the two SDE models. Model SDE 2 has the smaller BIC among the two SDE models. The standard deviations of all the microcirculation parameters are lower with model SDE2. The predictions $\hat{Q}_P$, $\hat{Q}_I$ and $\hat{S}$ obtained by the

Table 1: Estimated parameters and BIC criteria for the first dataset, using models ODE, SDE1 and SDE2. The values in parenthesis are the standard deviations evaluated using a numerical computation of the Fisher Information matrix.

	ODE model	SDE 1 model	SDE 2 model
F_T	51.56 (2.67)	51.56 (3.18)	51.56 (2.89)
V_b	40.01 (4.69)	40.01 (5.70)	40.01 (4.99)
PS	12.95 (3.77)	12.95 (4.55)	12.95 (3.81)
V_e	29.84 (2.22)	29.84 (2.56)	29.84 (2.02)
δ	7.20 (−−)	7.20 (−−)	7.20 (−−)
σ	8.06 (0.84)	7.93 **(0.19)**	7.93 **(0.00)**
σ_1	–	0.00 (0.00)	0.00 (0.88)
σ_2	–	0.00 (0.97)	–
BIC	931.82	941.50	936.63

Table 2: Estimated parameters and BIC for the second dataset, using models ODE, SDE1 and SDE2. The values in parenthesis are the standard deviations evaluated using a numerical computation of the Fisher Information matrix.

	ODE model	SDE 1 model	SDE 2 model
F_T	61.10 (4.06)	78.19 (3.15)	78.19 **(0.52)**
V_b	41.35 (5.41)	33.98 (5.55)	33.98 **(4.49)**
PS	6.90 (4.77)	11.88 (6.95)	11.88 **(5.46)**
V_e	16.79 (3.96)	18.75 (3.17)	18.75 **(2.95)**
δ	9.60 (−−)	**12.00** (−−)	**12.00** (−−)
σ	9.11 (0.81)	8.49 **(0.68)**	8.49 **(0.00)**
σ_1	–	1.08 (0.00)	1.08 (1.06)
σ_2	–	0.00 (1.23)	–
BIC	963.70	971.98	967.11

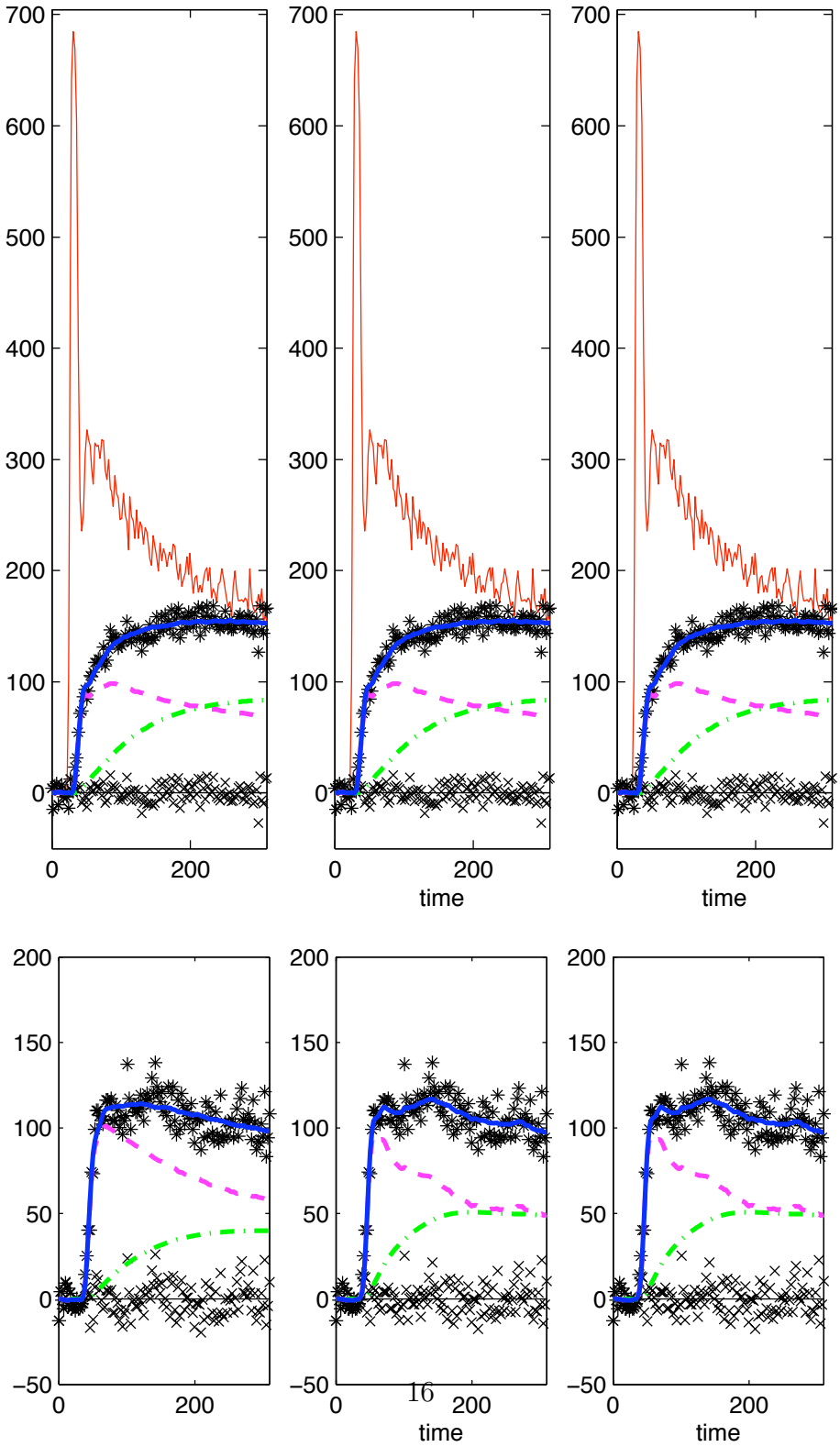

Figure 3: Predictions for real datasets 1 (top line) and 2 (bottom line), obtained with models ODE, SDE1 and SDE2 from left to right. Black stars ($*$) are the tissue observations (y_i), the AIF observations are represented by the red line for dataset 1, crosses ($\times$) are the residuals. The plain blue, dashed pink and dash-dotted green lines are respectively the predictions for $S(t)$, $Q_P(t)$ and $Q_I(t)$.

Table 3: Estimated parameters and BIC for dataset 3, using models ODE, SDE1 and SDE2. The values in parenthesis are the standard deviations evaluated using a numerical computation of the Fisher Information matrix.

	ODE model	SDE 1 model	SDE 2 model
F_T	22.40 (1.41)	17.54 (3.53)	17.55 (3.30)
V_b	36.09 (2.30)	45.23 (7.68)	45.18 (5.91)
PS	2.03 (0.56)	0.57 (5.77)	1.07 (5.86)
V_e	**63.91** (1.19)	0.03 (4.05)	0.06 (0.34)
δ	12.00 $(--)$	9.60 $(--)$	9.60 $(--)$
σ	7.69 (0.83)	6.51 **(0.00)**	6.51 **(0.00)**
σ_1	-	1.27 (0.66)	1.27 (0.95)
σ_2	-	0.03 (1.02)	-
BIC	937.82	925.32	920.46

ODE and the SDE estimations look quite different: SDE estimation achieves a better fit than ODE around times 90 and 130. Regarding the BIC criteria, the ODE model is the better model.

For dataset 3, the SDE predicted quantities of contrast agent in the interstitial compartment $\hat{Q}_I^{\text{SDE}}(t)$ was always null ($\hat{Q}_I^{\text{SDE}}(t) = 0 \quad \forall t \geq 0$) while the ODE prediction $\hat{Q}_I^{\text{ODE}}(t)$ was not (Figure 4). The ODE model detected exchanges inside the voxel between the two compartments. The ODE residuals were correlated, especially between times $t = 40$ and $t = 75$ contrary to the SDE residuals. The parameter estimates obtained by the ODE and the SDE models were different (Table 3). The two SDE estimated parameters are similar. The SDE1 estimated exchange volume ($\hat{V}_b^{\text{SDE}} = 0.03$) was statistically smaller than the ODE estimate ($\hat{V}_b^{\text{ODE}} = 63.91$). The SDE1 estimated permeability surface product ($\widehat{PS}^{\text{SDE}} = 0.57$) was much smaller than the ODE estimate ($\widehat{PS}^{\text{ODE}} = 2.03$). The estimation of σ_1 is different from 0 ($\hat{\sigma}_1^{\text{SDE}} = 1.27$). As $\hat{V}_b^{\text{ODE}} + \hat{V}_e^{\text{ODE}} = 100$ (see Table 3), the ODE estimation stopped at a boundary of the optimization domain (see Section 3.3). This led us to investigate the analysis further. By computing the ratio Q_P/AIF, we suspected that the ODE estimation was strongly influenced by the last observation times. Therefore we removed the last 3 (and then the last 5) observations. While the SDE estimation remained stable when removing observations (up to changes in the last digits), the ODE estimation changed totally. The results with the last 5 observations removed are added in Table 4. Figure 4 shows enhancement curves corresponding to the estimated pa-

Table 4: Estimated parameters and BIC for dataset 3 without the last 5 points, using models ODE, SDE1 and SDE2. The values in parenthesis are the standard deviations evaluated using a numerical computation of the Fisher Information matrix.

	ODE model	SDE 1 model	SDE 2 model
F_T	20.05 (0.00)	17.50 (3.23)	17.50 (3.47)
V_b	17.77 (0.00)	45.07 (3.99)	45.02 (6.38)
PS	**120.78** (0.00)	0.77 (0.00)	1.26 (6.26)
V_e	**15.75** (0.00)	0.04 (3.26)	0.06 (0.36)
δ	9.60 $(--)$	9.60 $(--)$	9.60 $(--)$
σ	8.10 (0.67)	6.37 (0.00)	6.37 (0.00)
σ_1	–	1.34 (0.47)	1.34 (0.98)
σ_2	–	0.03 (1.03)	–
BIC	897.99	888.04	883.21

rameters of Tables 3 and 4. Top curves are obtained with all data points by the ODE model (left) and the SDE models (right) corresponding to Table 3. In the SDE curves, the major part of the enhancement comes from the plasma while the interstitial enhancement is close to zero. Conversely, the ODE curves show enhancement from both plasma (dashed pink) and interstitium (dashdotted green). The bottom curves are obtained by the ODE model (left) and the SDE model (right) without the last 5 data points (right) corresponding to Table 4. On the bottom ODE curves, there is an inversion of curves (compared with the top left curves): the major part of enhancement is due to interstitium. Finally, the SDE2 model has the smaller BIC among the three models and is considered as the best model.

5. Simulated study

Simulations were performed to illustrate the properties of the estimators of the ODE and SDE models. The ODE and SDE estimators were those presented in the previous sections. The parameter values used for simulations were $F_T = 70$ ml min^{-1} 100 ml^{-1}, $V_b = 20$ %, $PS = 15$ ml min^{-1} 100 ml^{-1}, $V_e = 15$ %, $\delta = 9.6$ s and $\sigma = 7$ for the measurement error. First, a hundred data sets were simulated using the ODE model which corresponds to $\sigma_1 = \sigma_2 = 0$ in the SDE model. Parameters were estimated by the two methods. As shown in Table 5 (top), estimations by both methods were identical. Not surprisingly, the parameters σ_1 and σ_2 had very small

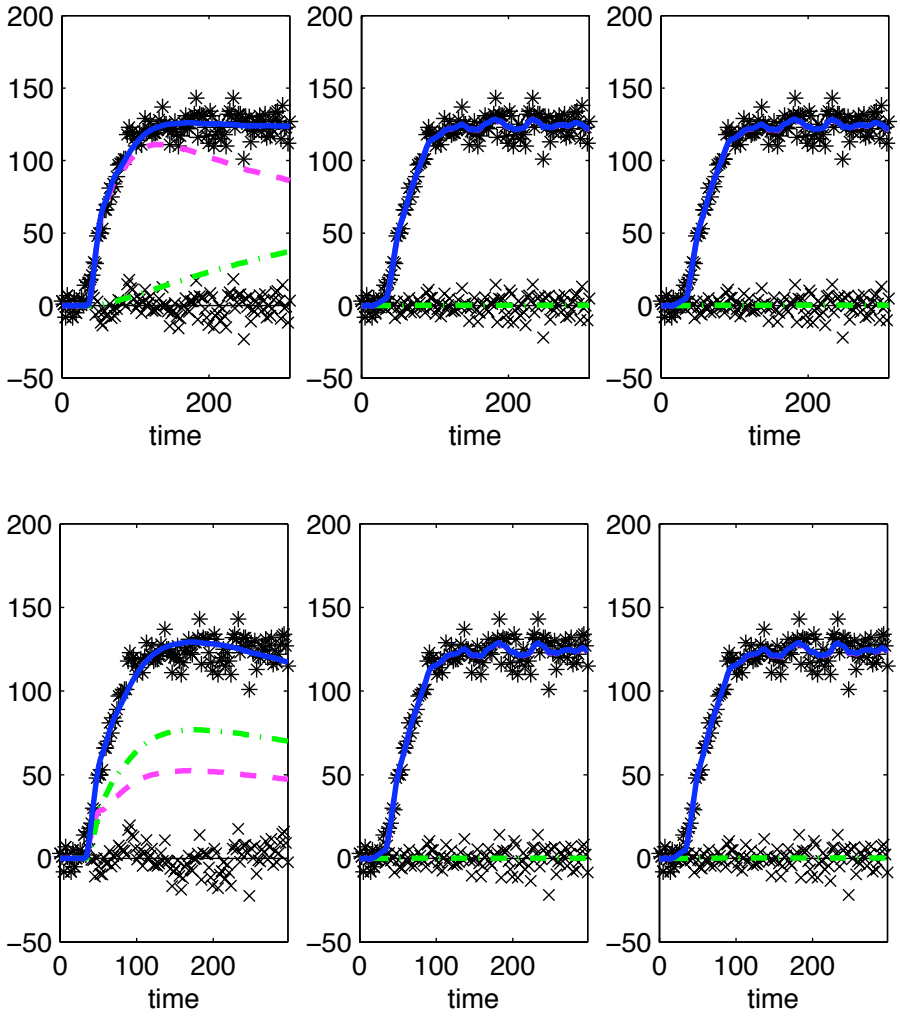

Figure 4: Top figures: predictions for real dataset 3, obtained with models ODE (left), SDE1, SDE2 and SDE3 from left to right. Black stars ($*$) are the tissue observations (y_i), crosses ($\times$) are the residuals. The plain blue, dashed pink and dash-dotted green lines are respectively the predictions for $S(t)$, $Q_P(t)$ and $Q_I(t)$. Bottom figures: predictions obtained when removing the last 5 observations.

SDE estimations. Then, a hundred data sets were simulated using the SDE model with $\sigma_1 = \sigma_2 = 2$. Results (Table 5, middle part) show a clear reduction of bias and standard deviations enlightening the advantage of the SDE estimation method. At last, a hundred data sets were simulated with $PS = 1$ (Table 5, bottom part), which corresponds to the case where the exchange between plasma and interstitium is small. We simulated a hundred data sets with the ODE model ($\sigma_1 = \sigma_2 = 0$) and a hundred data sets with the SDE model ($\sigma_1 = \sigma_2 = 1$). Note that the standard deviations (in parenthesis) are the empirical standard deviations computed from the 100 simulated datasets.

The SDE estimates are satisfactory. The delay δ was always estimated without bias. The ODE estimation of the parameters F_T and V_e were more biased than the SDE estimates. When the exchange between plasma and interstitium was small, the SDE estimates of V_e were less biased than the ODE estimates. The true value was $V_e = 15$. When the simulated model was ODE, the ODE estimate was $\widehat{V_e} = 27.01$ and the SDE estimate $\widehat{V_e} = 21.02$. When the simulated model was SDE, the ODE estimate was $\widehat{V_e} = 26.7$ and the SDE estimate $\widehat{V_e} = 17$. Again the SDE estimation seemed to be less sensitive to special value or data.

6. Discussion

To take into account noises which induce instability in microvascularization parameter estimation in DCE-MRI, a stochastic version of a two-compartment model described by stochastic differential equations was introduced. On voxels of normal female pelvises DCE-MRI data, both the stochastic and the standard deterministic two-compartment model (given by ordinary differential equations) were implemented. The stochastic model generally led to a more satisfactory description of enhancement curves and provided a more robust parameter estimation method.

When the permeability surface product (PS) was small, the ODE estimation method was unstable and gave different results when removing a few data points. Conversely, the stochastic method remained stable with or without these data. This proves that the stochastic method is less sensitive to special or sensitive data points (e.g. due to patient movements or measurement disturbances) and outperforms the ODE method. The parameter σ_2 is generally estimated close to 0 while σ_1 is not. As σ_1 appears in the

Table 5: Simulation study. Estimation results for three different sets of fixed parameters. Estimation when simulating under the ODE model (top part of the Table), when simulating under the SDE model ($\sigma_1 = \sigma_2 = 2$) (middle part of the Table) and when simulating with a small PS ($PS = 1$) under the SDE model ($\sigma_1 = \sigma_2 = 1$) (bottom part of the Table). Empirical means and standard deviations (in parenthesis) are computed for each estimated parameter from 100 simulated datasets analyzed by the ODE and the SDE estimations.

	F_T	V_b	PS	V_e	δ	σ	σ_1	σ_2
True par.	70	20	15	15	9.6	7	0	0
ODE est.	72.2	19.9	15.1	15.1	9.6	7.07	NA	NA
	(10)	(2.4)	(2.2)	(1.3)	(0)	(0.35)	NA	NA
SDE est.	72.2	19.9	15.1	15.1	9.6	6.99	0.03	0.002
	(10)	(2.4)	(2.2)	(1.3)	(0)	(0.35)	(0.12)	(0.015)
True par.	70	20	15	15	9.6	7	2	2
ODE est.	67.4	22	18.8	22.4	9.6	12.4	NA	NA
	(16)	(8.7)	(16)	(18)	(0)	(1.7)	NA	NA
SDE est.	71.9	21.7	15.3	17.3	9.6	6.88	2.54	1.22
	(15)	(6.6)	(9.8)	(13)	(0)	(0.51)	(0.69)	(0.84)
True par.	70	20	1	15	9.6	7	0	0
ODE est.	70.10	19.95	1.05	27.01	9.6	6.98	NA	NA
	(5.5)	(0.6)	(0.2)	(25.6)	(0)	(0.3)	NA	NA
SDE est.	70.09	19.9	1.05	21.2	9.6	6.91	0.07	0.716
	(5.4)	(0.6)	(0.2)	(25.8)	(0)	(0.3)	(0.2)	(0)
True par.	70	20	1	15	9.6	7	1	1
ODE est.	77.8	18.4	2.42	26.7	9.6	9.69	NA	NA
	(12)	(3.4)	(3)	(33)	(0)	(2.5)	NA	NA
SDE est.	72.4	19.7	2.08	17	9.6	6.89	1.32	0.716
	(10)	(2.5)	(2.5)	(26)	(0)	(0.32)	(0.52)	(0.43)

first equation of model (3), this reflects the measurement error in the AIF. Consequently, we recommend the use of the SDE model in this context.

These results were confirmed by the simulation study. For a given set of parameters $(F_T, V_b, PS, V_e,\ \delta, \sigma_1, \sigma_2, \sigma)$ and a given artificial arterial input function, a hundred trajectories were simulated under the stochastic model. For each of the hundred simulated trajectories, the parameters were estimated by both the ODE and SDE methods. The means of estimated parameters were globally close to the true values for both methods, with smaller variances for the SDE method. The parameters PS and V_e were closer to the true values with the SDE method than with the ODE method. The estimation of V_b was very similar with both methods, whatever the PS value. The estimation of F_T was similar with both methods when PS was large. On the contrary, for small PS, the estimation of F_T became biased with the ODE method and not with the SDE method.

The stochastic version of a classical multicompartment model is obtained by adding Brownian components to the deterministic model, leading to stochastic differential equations. Starting from a two-compartment exchange model with four parameters (tissue blood perfusion, tissue blood volume, permeability surface product, interstitial volume) and the bolus arrival time [19], we have built a SDE whose estimation method relies on maximum likelihood theory [15]. SDEs have been recently developed for medical applications in glucose dynamics [20], in neuron potential dynamics [21], in pharmacokinetics [22, 23], or in growth curve data [24]. These applications of SDEs show that stochastic versions of physiological models improve data fitting and stabilize parameter estimations. These results were confirmed in our study. Indeed, we obtained stable estimated parameters using a stochastic version of a complex parametric model while the deterministic model was giving results of high variability. The use of a stochastic model thus provides a serious improvement in data fitting and robustness in the estimation results even with a large number of parameters.

Yet, there are some limitations to our study. The two-compartment model does not take into account the blood propagation along capillaries, assumes instantaneous mixing into the interstitial compartment and equilibrium inside the interstitium of neighbor voxels. Moreover, the physiological parameters are assumed to be constant along time. Nevertheless, the good adjustment of enhancement curves, as measured by residuals, shows that this model is a reasonable physiological representation of tissue microcirculation even if it remains a crude approximation to true physiology. The model does

not hold true for all kinds of tissues. For instance, in the liver, the sinusoids are irrigated by a dual vascular system [25, 26] and in necrotic tissues without capillary network, the contrast enhancement is due to passive diffusion from adjacent irrigated tissues. However the present work could be extended by adapting models. We assume that the grey level variation is proportional to the total quantity of contrast agent inside the voxel. It might not always be true but it allows the analysis to be performed on the original data and simplifies the estimation procedure.

Some assumptions of the stochastic model may be criticized. For instance, constant variances for the Brownian motions may look unrealistic. It would be worth it to extend this work to SDE with variance functions of times or of contrast agent quantities. This would be to the price of additional mathematical difficulties. This work could also be extended to the case of non-Gaussian observation errors. For a unidimensional Markov chain (X_i) observed with non Gaussian errors, [27] proposes a quasi-maximum likelihood estimator based on the Kalman filter and shows the normality asymptotic distribution of this estimator. This approach can be extended to our bidimensional model. An additional assumption is the independence of the two Brownian motions, yielding easy interpretation. The extension to correlated Brownian motions is straightforward and does not affect the estimation procedure.

To conclude, this study shows that, in view of quantifying the tissue microcirculation parameters, the stochastic approach makes it possible to reduce the instability observed with the deterministic two-compartment model. By taking into account the sources of variations in DCE-MRI data, the SDE approach provides a more robust parameter extraction.

Acknowledgements This project was supported by a grant "Bonus Qualité Recherche" (BQR) from Université Paris Descartes.

References

[1] K. A. Miles, Functional CT imaging in oncology, Eur. Radiol. 13(5) (2003) 134–8.

[2] L. Ostergaard, Principles of cerebral perfusion imaging by bolus tracking., J Magn Reson Imaging 22 (2005) 710–717.

[3] S. Bisdas, G.-N. Konstantinou, P.-S. Lee, C.-H. Thng, J. Wagenblast, M. Baghi, T.-S. Koh, Dynamic contrast-enhanced CT of head and neck tumors: perfusion measurements using a distributed-parameter tracer

kinetic model. Initial results and comparison with deconvolution-based analysis., Phys Med Biol 52(20) (2007) 6181–96.

[4] V. Goh, A. R. Padhani, S. Rasheed, Functional imaging of colorectal cancer angiogenesis, Lancet Oncol. 8(3) (2007) 245–55.

[5] P.-S. Tofts, Modelling tracer kinetics in dynamic Gd-DTPA MR imaging, J Magn. Reson. Imaging 7 (1997) 91–101.

[6] L. Fournier, R. Thiam, C.-A. Cuénod, J. Medioni, L. Trinquart, D. Balvay, E. Banu, J. Balcaceres, G. Frija, S. Oudard, Dynamic contrast-enhanced CT (DCE-CT) as an early biomarker of response in metastatic renal cell carcinoma (mRCC) under anti-angiogenic treatment., J. of Clinical Oncology - ASCO Annual Meeting Proceedings (Post-Meeting Edition) 25.

[7] R. Jain, L. Scarpace, S. Ellika, L. Schultz, J. Rock, M. Rosenblum, S. Patel, T. Lee, T. Mikkelsen, First-pass perfusion computed tomography: initial experience in differentiating recurrent brain tumors from radiation effects and radiation necrosis, Neurosurgery 61 (2007) 778–86.

[8] M. Rosen, M. Schnall, Dynamic contrast-enhanced magnetic resonance imaging for assessing tumor vascularity and vascular effects of targeted therapies in renal cell carcinoma, Clin Cancer Res. 13(2) (2007) 770–6.

[9] A. Zhu, N. Holalkere, A. Muzikansky, K. Horgan, D. Sahani, Early antiangiogenic activity of bevacizumab evaluated by computed tomography perfusion scan in patients with advanced hepatocellular carcinoma, Oncologist 13 (2008) 120–5.

[10] G. Brix, F. Kiessling, R. Lucht, S. Darai, K. Wasser, S. Delorme, J. Griebel, Microcirculation and microvasculature in breast tumors: pharmacokinetic analysis of dynamic MR image series, Magn Reson Med. 52-2 (2004) 420–9.

[11] C. de Bazelaire, N. Siauve, L. Fournier, F. Frouin, P. Robert, O. Clement, E. de Kerviler, C. Cuenod, Comprehensive model for simultaneous MRI determination of perfusion and permeability using a blood-pool agent in rats rhabdomyosarcoma, Eur Radiol 15 (2005) 2497–505.

[12] R. Port, M. Knopp, G. Brix, Dynamic contrast-enhanced MRI using Gd-DTPA: interindividual variability of the arterial input function and consequences for the assessment of kinetics in tumors., Magn Reson Med 45 (2001) 1030–1038.

[13] G. Krishnamurthi, K.-M. Stantz, R. Steinmetz, V.-H. Gattone, C. Minsong, G.-D. Hutchins, L. Yun, Functional imaging in small animals using X-ray computed tomography: study of physiologic measurement reproducibility, IEEE Trans. on Medical Imaging 24(7) (2005) 832–43.

[14] C. Brochot, B. Bessoud, D. Balvay, C. Cuenod, N. Siauve, F. Bois, Evaluation of antiangiogenic treatment effects on tumors' microcirculation by bayesian physiological pharmacokinetic modeling and magnetic resonance imaging, Magn Reson Imaging. 24 (2006) 1059–1067.

[15] B. Favetto, A. Samson, Parameter estimation for a bidimensional partially observed Ornstein-Uhlenbeck process with biological application, Scand J Statist 37 (2010) 200–220.

[16] J. Bai, Least squares estimation of a shift in linear processes, Journal of Time Series Analysis 15 (5) (1994) 453–472.

[17] J. Stoer, R. Bulirsch, Introduction to numerical analysis, 2nd Edition, Vol. 12 of Texts in Applied Mathematics, Springer-Verlag, New York, 1993.

[18] I. Thomassin-Naggara, D. Balvay, E. Darai, M. Bazot, C. Cuenod, Dynamic contrast enhanced MR imaging to assess physiologic variations of myometrial perfusion, European Radiology 20 (2010) 984–994.

[19] D. Balvay, I. Tropres, R. Billet, A. Joubert, M. Peoc'h, C. Cuenod, G. Le Duc, Mapping the zonal organization of tumor perfusion and permeability in a rat glioma model by using dynamic contrast-enhanced synchrotron radiation CT., Radiology 250 (2009) 692–702.

[20] U. Picchini, S. Ditlevsen, A. De Gaetano, Maximum likelihood estimation of a time-inhomogeneous stochastic differential model of glucose dynamics, Mathematical Medicine and Biology 25 (2008) 141–155.

[21] H. Reinhard, K. Brodda, A stochastic model and a functional central limit theorem for information processing in large systems of neurons, J. Math. Biol. 52 (4) (2006) 439–457.

[22] S. Ditlevsen, K. Yip, N. Holstein-Rathlou, Parameter estimation in a stochastic model of the tubuloglomerular feedback mechanism in a rat nephron, Math Biosc 194 (2005) 49–69.

[23] S. Donnet, A. Samson, Parametric inference for mixed models defined by stochastic differential equations, ESAIM Probability & Statistics 12 (2008) 196–218.

[24] S. Donnet, J. Foulley, A. Samson, Bayesian analysis of growth curves using mixed models defined by stochastic differential equations, Biometrics 66 (2010) 733–741.

[25] C. Cuenod, I. Leconte, N. Siauve, A. Resten, C. Dromain, B. Poulet, F. Frouin, O. Clement, G. Frija, Early changes in liver perfusion caused by occult metastases in rats: detection with quantitative CT., Radiology 218 (2001) 556–561.

[26] R. Materne, A. Smith, F. Peeters, J. Dehoux, A. Keyeux, Y. Horsmans, B. Van Beers, Assessment of hepatic perfusion parameters with dynamic MRI., Magn Reson Med 47 (2002) 135–142.

[27] E. Ruiz, Quasi-maximum likelihood estimation of stochastic volatility models, Journal of econometrics 63 (1994) 289–306.